PRIVACY-PRESERVING DECENTRALIZED FEDERATED LEARNING VIA EXPLAINABLE ADAPTIVE DIFFERENTIAL PRIVACY

Fardin Jalil Piran
School of Mechanical, Aerospace, and Manufacturing Engineering
University of Connecticut
Storrs, CT 06269
fardin.jalil_piran@uconn.edu

Zhiling Chen
School of Mechanical, Aerospace, and Manufacturing Engineering
University of Connecticut
Storrs, CT 06269
zhiling.chen@uconn.edu

Yang Zhang
School of Mechanical, Aerospace, and Manufacturing Engineering
University of Connecticut
Storrs, CT 06269
yang.3.zhang@uconn.edu

Qianyu Zhou
School of Mechanical, Aerospace, and Manufacturing Engineering
University of Connecticut
Storrs, CT 06269
qianyu.zhou@uconn.edu

Jiong Tang
School of Mechanical, Aerospace, and Manufacturing Engineering
University of Connecticut
Storrs, CT 06269
jiong.tang@uconn.edu

Farhad Imani
School of Mechanical, Aerospace, and Manufacturing Engineering
University of Connecticut
Storrs, CT 06269
farhad.imani@uconn.edu

September 16, 2025

ABSTRACT

Decentralized federated learning faces privacy risks because model updates can leak data through inference attacks and membership inference, a concern that grows over many client exchanges. Differential privacy offers principled protection by injecting calibrated noise so confidential information remains secure on resource-limited IoT devices. Yet without transparency, black-box training cannot track noise already injected by previous clients and rounds, which forces worst-case additions and harms accuracy. We propose *PrivateDFL*, an explainable framework that joins hyperdimensional computing with differential privacy and keeps an auditable account of cumulative noise so each client adds only the difference between the required noise and what has already been accumulated. We evaluate on MNIST, ISOLET, and UCI-HAR to span image, signal, and tabular modalities, and we benchmark against transformer-based and deep learning-based baselines trained centrally with Differentially Private Stochastic Gradient Descent (DP-SGD) and Rényi Differential Privacy (RDP). PrivateDFL delivers higher accuracy, lower latency, and lower energy across IID and non-IID partitions while preserving formal (ϵ, δ) guarantees and operating without a central server. For example, under non-IID partitions, *PrivateDFL* achieves 24.42% higher accuracy than the Vision Transformer on MNIST while using about 10× less training time, 76× lower inference latency, and 11× less energy, and on ISOLET it exceeds Transformer accuracy by more than 80% with roughly 10× less training time, 40× lower inference latency, and 36× less training energy. Future work will extend the explainable accounting to adversarial clients and adaptive topologies with heterogeneous privacy budgets.

***K*eywords** Internet of Things · Decentralized Federated Learning · Differential Privacy · Explainable Artificial Intelligence · Hyperdimensional Computing

1 Introduction

The Internet of Things (IoT) is reshaping modern computing by interconnecting smart devices into one unified digital network. By 2025, this network is expected to include 80 billion devices [1], enabling unprecedented cyber-physical integration across autonomous systems, smart manufacturing, and urban infrastructure [2, 3]. However, this explosive

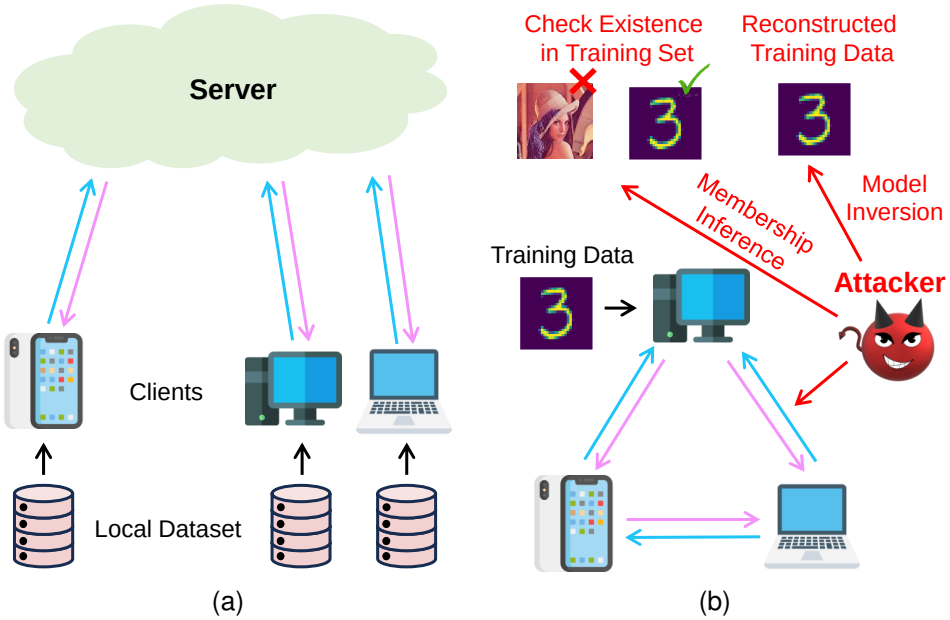

Figure 1: (a) Centralized federated learning framework, and (b) decentralized federated learning with potential data leakage through model inversion and membership inference attacks.

growth brings challenges such as data heterogeneity and the need for real-time, data-driven decision-making [4]. Traditional Machine Learning (ML) approaches, which rely on centralized architectures where raw data is sent to remote servers for training and inference, suffer from high latency, bandwidth constraints, and significant security and privacy vulnerabilities [5, 6]. Federated Learning (FL) has emerged as a promising paradigm to address issues by enabling collaborative model training while keeping data on local devices. In conventional Centralized Federated Learning (CFL), a central server aggregates client model updates, as shown in Fig. 1a, creating a single point of failure and heightened privacy risks [7]. Decentralized Federated Learning (DFL) removes this central server by allowing direct peer-to-peer communication, thereby enhancing scalability, reducing communication overhead, and improving privacy [8]. Nevertheless, DFL remains susceptible to sophisticated attacks. In a model inversion attack, an adversary can reconstruct sensitive training information from shared outputs or gradients [9]. In a membership inference attack, the adversary infers whether a particular record participated in training, as illustrated in Fig. 1b [10].

Several privacy-enhancing techniques have been explored to strengthen data protection in DFL. A common approach is anonymization, which obfuscates identifiable information to prevent individual records from being exposed. However, anonymization alone is insufficient against advanced inference attacks, such as model inversion, where adversaries reconstruct sensitive data even from anonymized outputs [9]. This issue is critical for high-dimensional datasets commonly found in decentralized learning, where anonymization fails to safeguard sensitive attributes. Homomorphic Encryption (HE) offers a more secure alternative by allowing encrypted data to be processed without decryption [11]. Despite its strong privacy guarantees, HE introduces significant computational overhead, making it impractical for large-scale federated models with resource-constrained IoT devices [12]. Another technique, Secure Multiparty Computation (SMC), enables multiple participants to collaboratively compute functions while preserving data privacy. However, SMC requires substantial communication and computation resources, limiting its applicability to real-world decentralized learning settings.

Differential Privacy (DP) has emerged as a fundamental approach to mitigating privacy risks in DFL. By injecting controlled noise into model updates, DP reduces vulnerabilities such as model inversion and membership inference attacks, thereby safeguarding individual contributions during collaborative training [13–15]. Proper calibration of noise ensures that individual data points exert minimal influence on model outputs, striking a balance between privacy and utility [16, 17]. In decentralized environments, maintaining this balance is particularly challenging. When too much noise is added, the resulting accumulation severely reduces model accuracy, whereas adding too little noise exposes the system to privacy risks [18].

As illustrated in Fig. 2, the noise level plays a decisive role in preserving both privacy and utility. When the noise is too high, reconstructed samples resemble random patterns rather than the original data, effectively protecting privacy

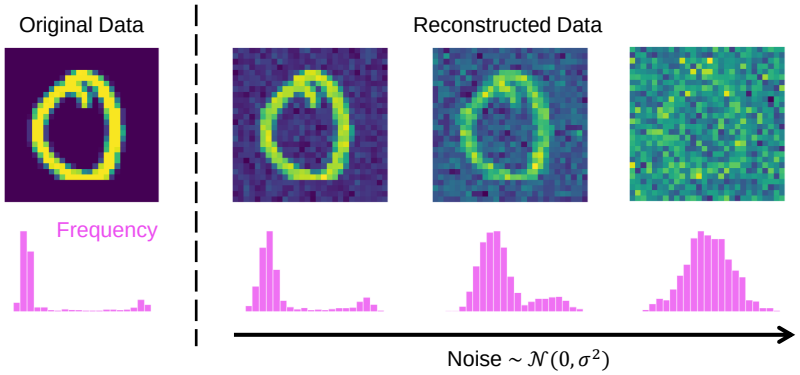

Figure 2: Reconstruction of a secure data point.

but rendering the data distribution unusable for training. In contrast, when the noise is too low, the distribution of secure samples remains close to the original data, which preserves accuracy but makes it easier for adversaries to reconstruct sensitive information. These results underscore the importance of tuning privacy parameters carefully in DFL environments.

Building on this observation, standard black-box DFL cannot track the DP noise already injected by earlier clients and rounds, so each client assumes a worst-case exposure and readds a full dose of noise. This over-conservative behavior inflates variance and diminishes utility. We close this gap with an eXplainable AI (XAI)-guided noise accountant that keeps an auditable tally of cumulative noise and, at each step, adds only the incremental amount needed to meet the current privacy target, namely the difference between the required noise and what is already present. This mechanism preserves formal privacy guarantees while maintaining accuracy, and it renders the effect of noise on model updates transparent, enabling trustworthy deployment in safety-critical contexts [19].

We present Private Decentralized Federated Learning (*PrivateDFL*), an XAI-driven framework that enhances privacy, interpretability, and security in DFL. As shown in Fig. 3, PrivateDFL uses explainability to reveal how privacy mechanisms behave during training and to keep model updates auditable. Clients are arranged on a ring so that each device updates a HyperDimensional computing (HD) model with its local data and then passes the model to the next peer. The key contribution is an adaptive noise controller under DP. Rather than injecting a constant noise level at every iteration, each client tracks the cumulative privacy noise across rounds and adjusts subsequent noise to account for prior contributions. This XAI-guided policy preserves strong privacy while avoiding unnecessary losses in accuracy. Our contributions in this paper are summarized as follows:

- We present PrivateDFL, an XAI framework that improves interpretability and transparency in privacy-preserving DFL by coupling explainability with DP-constrained model training.
- We propose an adaptive privacy mechanism that uses XAI to track cumulative noise across rounds, preventing overestimation of DP noise and tuning privacy and utility tradeoffs in serverless FL.
- We show that PrivateDFL dynamically regulates noise to limit performance loss and increase robustness, enabling reliable decentralized learning in real-world deployments.

The remainder of this paper is structured as follows: Section 2 reviews existing DFL frameworks, examines DP as a mechanism for safeguarding ML models in FL, and explores the integration of HD with DP. Section 3 introduces fundamental concepts related to HD, and DP, then details the proposed PrivateDFL framework and its implementation. Section 4 outlines the experimental setup, and the results of the experiments are presented and analyzed in Section 5, where PrivateDFL is evaluated in terms of privacy, accuracy, and efficiency. Finally, Section 6 summarizes the contributions of this work in developing trustworthy, explainable, and privacy-preserving decentralized learning models, while proposing future research directions for advancing XAI approaches in secure IoT deployments.

2 Research Background

2.1 Decentralized Federated Learning

While CFL frameworks enable privacy-preserving model training, they face challenges such as managing client heterogeneity [20], limited communication resources [21], and high computational demands [22]. Additionally,

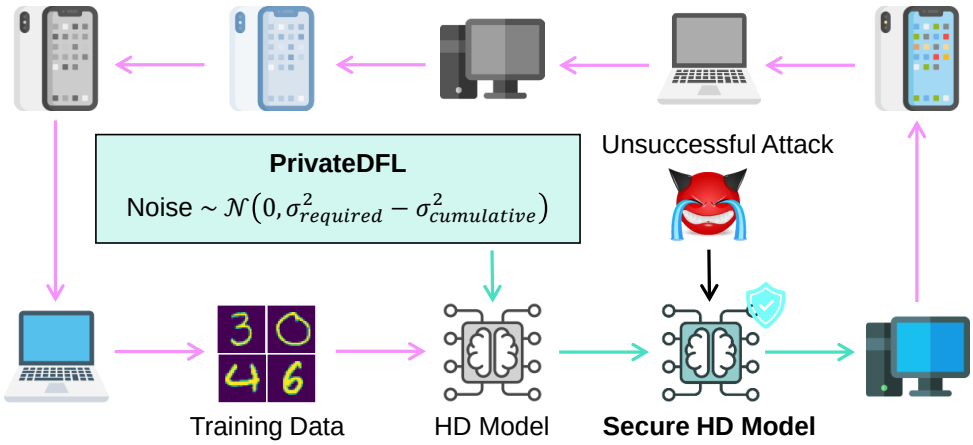

Figure 3: Overview of the PrivateDFL model.

fairness, security, and reliability concerns, such as vulnerability to malicious attacks and central server dependency, can undermine CFL's effectiveness [23–25]. These limitations highlight the need for DFL, which can mitigate these shortcomings by eliminating the single point of failure and enhancing system robustness.

Several DFL frameworks have been proposed to enable FL without reliance on a central server. Fully DFL, introduced by Lalitha et al. [26], eliminates the need for a global aggregator by allowing direct communication between clients, forming a peer-to-peer structure. Decentralized federated averaging, proposed by Lian et al. [27], extends the federated averaging algorithm to a decentralized setting, where clients update their models through local exchanges with neighboring nodes. Blockchain-based DFL incorporates blockchain technology to ensure secure, tamper-resistant model aggregation without a central server [28]. Additionally, graph-based FL structures client interactions as a graph topology, enabling efficient aggregation based on local neighborhoods [8]. These frameworks leverage decentralized optimization strategies to enhance scalability, fault tolerance, and robustness, making them suitable for distributed and resource-constrained environments such as IoT networks.

These DFL frameworks facilitate the distribution of the learning process among clients without transmitting raw data, thereby safeguarding confidential information. However, they remain vulnerable to model inversion and membership inference attacks, where adversaries attempt to reconstruct training data from shared model updates. Such privacy threats necessitate the integration of DP to provide formal privacy guarantees and mitigate data leakage risks. Ensuring privacy in DFL while maintaining model utility remains a key challenge, further motivating the need for adaptive privacy-preserving mechanisms that dynamically regulate noise and enhance security in decentralized learning environments.

2.2 Differential Privacy

DP, introduced by Dwork et al. [29], offers a rigorous framework for protecting data by injecting carefully calibrated noise into computations. With DP, the distribution of an algorithm's outputs changes only slightly when any single record is added or removed, ensuring that individual contributions are indistinguishable and thus protected. This mechanism reduces the effectiveness of reconstruction and presence-testing attacks, including model inversion and membership inference, and is therefore central to privacy-preserving ML. A prominent approach for applying DP in learning is Differentially Private Stochastic Gradient Descent (DP-SGD), which augments standard SGD with per-example gradient clipping and noise added to aggregated gradients during training. When properly tuned, DP-SGD provides quantifiable privacy guarantees while maintaining useful model performance [30].

Rényi Differential Privacy (RDP) extends the DP framework by quantifying privacy loss through Rényi divergence [31]. In contrast to classical DP accounting with rigid worst-case bounds, RDP offers a more flexible composition tool for tracking cumulative privacy over many queries. This property aligns well with iterative training procedures such as SGD, where successive steps gradually consume the privacy budget. By selecting the divergence order and converting RDP guarantees to the (ϵ, δ)-DP form, practitioners can calibrate noise more precisely and achieve a finer privacy–utility trade-off. The added mathematical machinery, however, can complicate practical adoption.

Prior research has integrated DP into FL to bolster security and protect client data. Gong et al. combined DP with HE to shield gradient updates from a central server, yet completely preventing leakage remains difficult [32]. Wu et al. applied DP to multi-task FL by injecting Gaussian noise into model parameters, but the defense remains vulnerable to threats

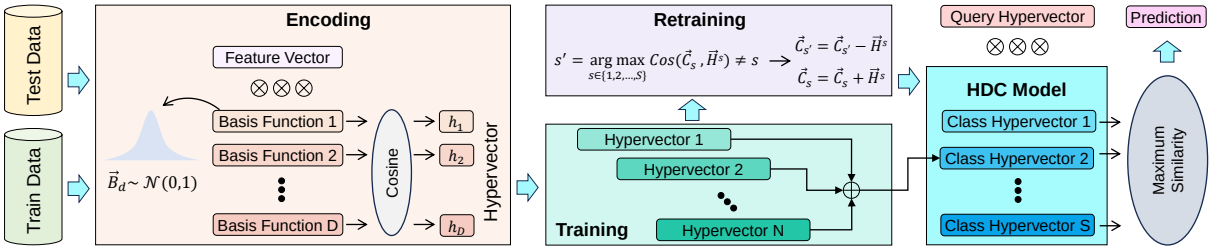

Figure 4: Overview of the HD model.

such as model inversion and label-flipping [33]. Cyffers et al. investigated a decentralized scheme using a relaxed form of local DP that supports efficient analysis while balancing privacy and utility [16]; nevertheless, decentralization can increase susceptibility to data poisoning and other adversarial attacks [34]. Tran et al. introduced a secure decentralized protocol in which the master role rotates among clients, removing the fixed central server [35], although collusion among participants can still compromise the system [34].

Hybrid approaches that pair DP with complementary security mechanisms aim to strengthen privacy in decentralized learning. Zhao et al. proposed sharing only partial gradients with Gaussian perturbations while relaying updates through an intermediary proxy to obscure client identity [36]. Although anonymity improves, robustness against inference attacks remains insufficiently assessed. Yin et al. combined functional encryption with a Bayesian DP formulation to secure communications in federated settings [37], yet reliance on a trusted third party creates an additional attack surface and may still permit model inversion. Other studies adapt noise through encoding strategies that respond to the underlying data distribution, seeking to curb utility loss while maintaining privacy [38]. For cyber-physical systems, privacy has been pursued by injecting random noise to anonymize signals, which can degrade data fidelity [39]. Three-way attribute-decision methods have also shown promise for IoT by structuring sensitive features prior to applying DP, improving protection without excessive performance penalties [40].

Recent studies increasingly emphasize the role of XAI in privacy-aware FL. By coupling interpretability techniques with ML-based privacy mechanisms, XAI improves transparency while reinforcing security. Zheng et al. introduced a dynamic privacy-budget scheme that uses explanatory signals to gauge workload sensitivity and adjust noise accordingly [41]. Incorporating XAI in DP pipelines enables more interpretable and efficient privacy management. As decentralized learning advances, a central challenge is to develop adaptive privacy methods with formal, verifiable guarantees for trustworthy AI.

2.3 Hyperdimensional Computing

Efforts to incorporate privacy-preserving techniques into HD models have gained attention in recent years. Hernandez-Cano et al. [42] proposed an intelligent noise-injection strategy that masks less critical features in the original feature space, though the work did not determine the precise noise levels needed for formal privacy guarantees. Khaleghi et al. [43] integrated DP into HD frameworks to strengthen security but did not evaluate the resulting trade-offs in model accuracy. Piran et al. [44] examined the influence of DP on HD models with an emphasis on explainability, analyzing how varying noise levels affect performance, but their study did not extend to federated settings. In subsequent work, Piran et al. [45] introduced DP noise management within an HD-based CFL framework; however, their design relied on a centralized server for aggregation, reducing the overall privacy benefits. These gaps underscore the importance of advancing methods that improve both the transparency and interpretability of HD models in DFL. A promising research direction is the design of adaptive noise-injection schemes that maintain a balance between strong privacy guarantees and high model accuracy.

3 Research Methodology

3.1 Hyperdimensional Computing

HD is an XAI framework that enhances interpretability in ML by leveraging high-dimensional vector representations, known as hypervectors [46, 47]. Inspired by brain-like cognitive mechanisms, HD computing encodes and manipulates information in a distributed and interpretable manner [48]. Unlike traditional ML models that rely solely on numerical optimization, HD computing supports robust pattern recognition while maintaining explainability through structured vector operations [44]. As illustrated in Fig. 4, the HD framework proceeds through four main stages, namely encoding,

training, inference, and retraining. Together, these stages integrate representation learning with interpretability, making HD computing suitable for privacy-preserving and explainable decentralized systems [45].

Encoding transforms input features into high-dimensional hypervectors, where each dimension equally contributes to data representation. Given a feature vector $\vec{F}$, the encoding process maps it into a hypervector $\vec{H}$ using a set of random basis functions $\{\vec{B}_d\}_{d=1}^{D}$ sampled from $\mathcal{N}(0,1)$, such that each hypervector component is computed as $h_d = \cos(\vec{F} \cdot \vec{B}_d)$. This approach enables an interpretable representation that preserves structural similarities in the data, while providing robustness for privacy-preserving and explainable learning applications.

Training builds class representations by aggregating hypervectors with the same label. Let $\vec{H}^s$ denote an encoded sample belonging to class s. For class s, the class hypervector $\vec{C}_s$ is computed as the sum of all such hypervectors

$$\vec{C}_s = \sum \vec{H}^s \tag{1}$$

By merging multiple hypervectors, the HD model produces a high-dimensional prototype that captures common patterns and variations within each class. This aggregation not only improves classification accuracy but also provides an interpretable structure that helps explain how features contribute to the class representation, while remaining robust against noise and variability in the data.

Inference assigns a query hypervector $\vec{H}^q$ to a class by comparing it with the stored class hypervectors. The classification decision is made using the cosine similarity function, defined as

$$\text{Cos}(\vec{C}_s, \vec{H}^q) = \frac{\vec{C}_s \cdot \vec{H}^q}{||\vec{C}_s|| \cdot ||\vec{H}^q||}, \tag{2}$$

which measures the alignment between $\vec{H}^q$ and each class hypervector $\vec{C}_s$. The predicted class is then determined by selecting the index with the maximum similarity score:

$$q = \underset{s \in \{1,2,\ldots,S\}}{\arg\max} \ \text{Cos}(\vec{C}_s, \vec{H}^q). \tag{3}$$

The class q is selected as the final prediction. This similarity-based process provides an interpretable decision rule, making it possible to trace how a query is matched to class prototypes, thereby improving explainability in decentralized learning.

Retraining refines class hypervectors to improve adaptability when new evidence is observed. If a query hypervector is misclassified, the model updates its class representations through corrective adjustments:

$$\begin{aligned} \vec{C}_{s'} &= \vec{C}_{s'} - \vec{H}^s, \\ \vec{C}_s &= \vec{C}_s + \vec{H}^s. \end{aligned} \tag{4}$$

This adjustment strengthens the correct class representation while weakening the influence of incorrect associations, making the decision boundaries more interpretable. By continuously adapting class hypervectors, the HD model improves accuracy and preserves stability in evolving data environments. Leveraging distributed high-dimensional representations and lightweight operations, this process provides a scalable and energy-efficient approach, particularly well-suited for decentralized learning where explainability, robustness, and privacy are critical.

3.2 Differential Privacy

DP provides a rigorous guarantee that the inclusion or removal of any single record has only a limited effect on the output of a computation. This protection is achieved by adding calibrated random noise to model updates. Two parameters, ϵ and δ, define the strength of the guarantee. The privacy budget ϵ controls the maximum change in the output distribution when one record is modified, so smaller values of ϵ yield stronger privacy. The parameter δ represents a small probability that the guarantee may fail, and it is usually set to be negligibly small.

Definition 1 *A randomized mechanism $\mathcal{M}$ satisfies (ϵ, δ)-DP if, for any pair of neighboring datasets I_1 and I_2 that differ in one record,*

$$\Pr[\mathcal{M}(I_1)] \leq e^{\epsilon} \Pr[\mathcal{M}(I_2)] + \delta. \tag{5}$$

This condition ensures that individual records cannot be reliably distinguished from the outputs of the mechanism.

Definition 2 *The Gaussian Mechanism achieves (ϵ, δ)-DP by perturbing the output of a function $g(I)$ with Gaussian noise of variance σ_{dp}^2:*

$$\mathcal{M}(I) = g(I) + \mathcal{N}(0, \sigma_{dp}^2). \tag{6}$$

This approach reduces the chance that an adversary can infer sensitive information about any individual in the dataset.

Definition 3 *The sensitivity Δg of a function g is defined as*

$$\Delta g = \max_{I_1, I_2} \|g(I_1) - g(I_2)\|, \tag{7}$$

which represents the maximum possible change in the function's output when one record is modified.

Theorem 1 *The Gaussian Mechanism satisfies (ϵ, δ)-DP if the variance of the added noise satisfies*

$$\sigma_{dp}^2 \geq 2\frac{\Delta g^2}{\epsilon^2} \ln\left[\frac{1.25}{\delta}\right]. \tag{8}$$

These foundations provide a balance between privacy and accuracy, making DP a practical choice for decentralized learning in dynamic and resource-constrained environments.

3.3 PrivateDFL

Building on the foundations of decentralized learning, HD, and DP, we introduce PrivateDFL, a secure IoT framework that unifies these three components to enable privacy-preserving model training. Within this framework, HD provides the representational basis for interpretable and robust classification, while DFL eliminates the central server by allowing clients to collaboratively update and exchange HD models in sequence. To protect individual contributions during this process, DP is employed with privacy parameters (ϵ, δ). Following standard practice, δ is chosen to be smaller than the inverse of the total number of training samples N, such that $\delta = \delta_0/N$ with $\delta_0 \in (0, 1)$. We compute the noise that client k at each communication round r will add to the HD model, $\vec{\Gamma}_k^r$, by computing the diffence between required noise to secure HD model by client k at communication round r, $\vec{\xi}_k^r$, and the cumulative noise recived from the previose client over all prevois rounds, $\vec{\Psi}_{k-1}^r$.

Training begins with the collaborative construction of the HD model. The first client generates class hypervectors using Equation (1), perturbs them with DP noise as specified in Theorem 2, and forwards the secure HD model to the next participant, with validity established in Proof 1. Each subsequent client then receives the noisy class hypervectors, forms its own class hypervectors from local data, merges them with the received model, and adds further noise before transmission. The precise calibration of this additional noise is defined in Theorem 3 and justified in Proof 2.

Theorem 2 *The DP noise added to the HD model by the first client in the first round is*

$$\vec{\Gamma}_1^1 \sim \mathcal{N}\left(0, \frac{2D}{\epsilon^2} \ln\left[\frac{1.25N}{\delta_0}\right]\right). \tag{9}$$

Proof 1 *The required noise $\vec{\xi}_1^1$ for the first client is obtained from Equation* (8)*. From Equation* (7)*, the sensitivity of the model is $\Delta g = \sqrt{D}$, since hypervector elements lie in the bounded interval $[-1, 1]$ (attaining ± 1 at the extrema), and the largest possible difference between two neighboring datasets yields an ℓ_2-norm of $\sqrt{D}$.*

In the worst case, all N training samples for a given client contribute to a single class hypervector. Thus, we set $\delta = \delta_0/N$. Substituting into Equation (8) *gives*

$$\vec{\xi}_1^1 \sim \mathcal{N}\left(0, \frac{2D}{\epsilon^2} \ln\left[\frac{1.25N}{\delta_0}\right]\right). \tag{10}$$

Since this is the first round with no previously accumulated noise,

$$\vec{\Gamma}_1^1 = \vec{\xi}_1^1. \tag{11}$$

Theorem 3 *For any client $k \geq 2$ in the first round, the DP noise added to the HD model satisfies*

$$\vec{\Gamma}_k^1 \sim \mathcal{N}\left(0, \frac{2D}{\epsilon^2} \ln\left[\frac{k}{k-1}\right]\right), \tag{12}$$

where k denotes the client index.

Proof 2 *From Equation* (8) *and the sensitivity in Equation* (7) *with* $\Delta g = \sqrt{D}$*, the cumulative noise required after client* k *in round 1 is*

$$\vec{\xi}_k^1 \sim \mathcal{N}\left(0, \frac{2D}{\epsilon^2} \ln\left[\frac{1.25\, k\, N}{\delta_0}\right]\right), \tag{13}$$

using $\delta = \delta_0/(kN)$ *in the worst case. The model received from client* $k-1$ *already contains*

$$\vec{\Psi}_{k-1}^1 \sim \mathcal{N}\left(0, \frac{2D}{\epsilon^2} \ln\left[\frac{1.25\,(k-1)\, N}{\delta_0}\right]\right). \tag{14}$$

Choose $\vec{\Gamma}_k^1$ *independent of* $\vec{\Psi}_{k-1}^1$ *so that* $\vec{\Psi}_{k-1}^1 + \vec{\Gamma}_k^1$ *attains the target variance. Then*

$$\begin{aligned}\vec{\Gamma}_k^1 &\sim \mathcal{N}\left(0, \frac{2D}{\epsilon^2}\left(\ln\left[\tfrac{1.25\, k\, N}{\delta_0}\right] - \ln\left[\tfrac{1.25\,(k-1)\, N}{\delta_0}\right]\right)\right) \\ &= \mathcal{N}\left(0, \frac{2D}{\epsilon^2} \ln\left[\frac{k}{k-1}\right]\right).\end{aligned} \tag{15}$$

In subsequent communication rounds, each client refines the received class hypervectors using Equation (4) with its own private training data. It then calibrates additional DP noise by accounting for the perturbations accumulated in earlier rounds to meet the privacy constraints, and forwards the secure HD model to the next participant. The noise schedule for the first client in these rounds is stated in Theorem 4 and justified in Proof 3, while the schedule for the remaining clients is given in Theorem 5 and justified in Proof 4.

Theorem 4 *The DP noise added by the first client in round* r *after* $r-1$ *prior communication rounds is*

$$\vec{\Gamma}_1^r \sim \mathcal{N}\left(0, \frac{2D}{\epsilon^2} \ln\left[\frac{K(r-1)+1}{K(r-1)}\right]\right). \tag{16}$$

Proof 3 *Let* $\vec{\xi}_1^r$ *denote the cumulative noise required to protect all contributions present when the first client completes round* r*, and let* $\vec{\Psi}_K^{r-1}$ *be the accumulated noise already contained in the model received from client* K *after* $r-1$ *rounds. By Equation* (7)*, the sensitivity remains* $\Delta g = \sqrt{D}$*. In round* r*, the model aggregates* $KN(r-1)+N$ *samples, hence*

$$\delta = \frac{\delta_0}{KN(r-1)+N}. \tag{17}$$

Substituting into Equation (8) *yields*

$$\vec{\xi}_1^r \sim \mathcal{N}\left(0, \frac{2D}{\epsilon^2} \ln\left[\frac{1.25\, KN(r-1) + 1.25\, N}{\delta_0}\right]\right). \tag{18}$$

The received model already contains

$$\vec{\Psi}_K^{r-1} \sim \mathcal{N}\left(0, \frac{2D}{\epsilon^2} \ln\left[\frac{1.25\, KN(r-1)}{\delta_0}\right]\right). \tag{19}$$

Choose $\vec{\Gamma}_1^r$ *independent of* $\vec{\Psi}_K^{r-1}$ *so that their sum attains the target variance. Therefore,*

$$\begin{aligned}\vec{\Gamma}_1^r &\sim \mathcal{N}\left(0, \frac{2D}{\epsilon^2}\left(\ln\left[\tfrac{1.25\, KN(r-1)+1.25\, N}{\delta_0}\right] - \ln\left[\tfrac{1.25\, KN(r-1)}{\delta_0}\right]\right)\right) \\ &= \mathcal{N}\left(0, \frac{2D}{\epsilon^2} \ln\left[\frac{K(r-1)+1}{K(r-1)}\right]\right).\end{aligned} \tag{20}$$

Theorem 5 *For client* $k \in \{2, \ldots, K\}$ *in round* r*, after* $k-1$ *clients have updated the class hypervectors, the DP noise added to the HD model is*

$$\vec{\Gamma}_k^r \sim \mathcal{N}\left(0, \frac{2D}{\epsilon^2} \ln\left[\frac{K(r-1)+k}{K(r-1)+k-1}\right]\right). \tag{21}$$

Proof 4 *By Equation* (7)*, the sensitivity is* $\Delta g = \sqrt{D}$*. When client* k *completes round* r*, the model aggregates* $KN(r-1)+kN$ *samples, so* $\delta = \delta_0/(KN(r-1)+kN)$*. Hence*

$$\vec{\xi}_k^r \sim \mathcal{N}\left(0, \frac{2D}{\epsilon^2} \ln\left[\frac{1.25\,(K(r-1)+k)N}{\delta_0}\right]\right), \tag{22}$$

and the received model already contains

$$\vec{\Psi}_{k-1}^r \sim \mathcal{N}\left(0, \frac{2D}{\epsilon^2} \ln\left[\frac{1.25\,(K(r-1)+k-1)N}{\delta_0}\right]\right). \tag{23}$$

Choose $\vec{\Gamma}_k^r$ *independent of* $\vec{\Psi}_{k-1}^r$ *so that their sum attains the target variance. Therefore,*

$$\begin{aligned}\vec{\Gamma}_k^r &\sim \mathcal{N}\left(0, \frac{2D}{\epsilon^2}\left(\ln\left[\tfrac{1.25\,(K(r-1)+k)N}{\delta_0}\right] - \ln\left[\tfrac{1.25\,(K(r-1)+k-1)N}{\delta_0}\right]\right)\right) \\ &\sim \mathcal{N}\left(0, \frac{2D}{\epsilon^2} \ln\left[\frac{K(r-1)+k}{K(r-1)+k-1}\right]\right).\end{aligned} \tag{24}$$

The added noise in each communication round is determined by Theorems 2–5. For the first round, the noise for the initial client is given in Theorem 2 (Equation 9), while the noise for clients $k \geq 2$ is described in Theorem 3 (Equation 12). In subsequent rounds ($r \geq 2$), the noise for the first client is defined in Theorem 4 (Equation 16), and for all other clients in that round it is specified by Theorem 5 (Equation 21). It is straightforward to observe that Equation 16 can be obtained from Equation 21 by setting $k = 1$. Similarly, Equation 12 is obtained from Equation 21 by substituting $r = 1$. Therefore, the noise injection procedure simplifies to the following rule. The first client in the first round follows Theorem 2. All other cases, including clients $k \geq 2$ in the first round and all clients in subsequent rounds, follow Theorem 5. The implementation of PrivateDFL based on this unified formulation is presented in Algorithm 1.

3.4 Cumulative Noise

In this section, we analyze the cumulative noise generated under the proposed PrivateDFL framework for each communication round and compare it with the required noise needed to protect all training samples up to that round. To further highlight the benefit of PrivateDFL, we also contrast it with a black-box scenario, where noise contributions from previous clients and earlier communication rounds cannot be tracked, resulting in excessive noise being added to the HD model. We denote by $\vec{\gamma}_r^k$ the cumulative noise after client k at round r under PrivateDFL, where prior contributions are explicitly accounted for. In contrast, $\vec{\Xi}_K^r$ represents the cumulative noise in the black-box setting, where past noise cannot be traced and the system redundantly adds new noise at each step.

For the first communication round, the noise applied by the first client is the same under both PrivateDFL and the black-box scenario. In this case, the required amount of noise is exactly satisfied, ensuring that the HD model is secured in either formulation. Formally, the cumulative noise $\vec{\gamma}_1^1$ in PrivateDFL and the cumulative noise $\vec{\Xi}_1^1$ in the black-box case coincide:

$$\vec{\gamma}_1^1 = \vec{\Gamma}_1^1 \sim \mathcal{N}\left(0, \frac{2D}{\epsilon^2} \ln\left[\tfrac{1.25N}{\delta_0}\right]\right) = \vec{\xi}_1^1, \tag{25}$$

$$\vec{\Xi}_1^1 = \vec{\xi}_1^1 \sim \mathcal{N}\left(0, \frac{2D}{\epsilon^2} \ln\left[\tfrac{1.25N}{\delta_0}\right]\right) = \vec{\gamma}_1^1. \tag{26}$$

Algorithm 1 PrivateDFL: Private Decentralized Federated Learning

Input $\{\vec{F}_k\}_{k=1}^{K}$ ▷ Training samples from K clients
Output $\{\tilde{\vec{C}}_{s,K}^{R}\}_{s=1}^{S}$ ▷ Final secure HD model after R rounds (state at client K)
Encoding $\vec{H} = (\cos(\vec{F}\cdot\vec{B}_d))_{d=1}^{D}$, $\{\vec{B}_d\}_{d=1}^{D} \sim \mathcal{N}(0,1)$
ClassHV $\vec{C}_s = \sum \vec{H}^s,\ s = 1{:}S$
Retrain $\vec{C}_{s'} \leftarrow \vec{C}_{s'} - \vec{H}^s$, $\vec{C}_s \leftarrow \vec{C}_s + \vec{H}^s$
for $r = 1{:}R$ **do**
  for $k = 1{:}K$ **do**
    if $r = 1 \wedge k = 1$ **then**
      $\vec{\Gamma}_1^1 \sim \mathcal{N}\Big(0, \frac{2D}{\epsilon^2}\ln\Big[\frac{1.25N}{\delta_0}\Big]\Big)$
      $\{\tilde{\vec{C}}_{s,1}^{1}\}_{s=1}^{S} \leftarrow \text{ClassHV}(\text{Encoding}(\vec{F}_1)) + \vec{\Gamma}_1^1$
    else if $r = 1 \wedge k \neq 1$ **then**
      $\vec{\Gamma}_k^r \sim \mathcal{N}\Big(0, \frac{2D}{\epsilon^2}\ln\Big[\frac{K(r-1)+k}{K(r-1)+k-1}\Big]\Big)$
      $\{\tilde{\vec{C}}_{s,k}^{1}\}_{s=1}^{S} \leftarrow \{\tilde{\vec{C}}_{s,k-1}^{1}\}_{s=1}^{S} + \text{ClassHV}(\text{Encoding}(\vec{F}_k)) + \vec{\Gamma}_k^1$
    else
      $\vec{\Gamma}_k^r \sim \mathcal{N}\Big(0, \frac{2D}{\epsilon^2}\ln\Big[\frac{K(r-1)+k}{K(r-1)+k-1}\Big]\Big)$
      $\{\tilde{\vec{C}}_{s,k}^{r}\}_{s=1}^{S} \leftarrow \text{Retrain}\big(\{\tilde{\vec{C}}_{s,k-1}^{r}\}_{s=1}^{S}, \text{Encoding}(\vec{F}_k)\big) + \vec{\Gamma}_k^r$
    end if
  end for
  if $r < R$ **then**
    $\{\tilde{\vec{C}}_{s,1}^{r+1}\}_{s=1}^{S} \leftarrow \{\tilde{\vec{C}}_{s,K}^{r}\}_{s=1}^{S}$
  end if
end for
return $\{\tilde{\vec{C}}_{s,K}^{R}\}_{s=1}^{S}$

For clients $k \geq 2$ in the first round, the cumulative noise at client k under PrivateDFL equals the required noise to protect the union of samples from the first k clients:

$$\begin{aligned}
\vec{\gamma}_k^1 &= \sum_{i=1}^{k} \vec{\Gamma}_i^1 \\
&\sim \mathcal{N}\left(0, \frac{2D}{\epsilon^2}\left(\ln\Big[\frac{1.25N}{\delta_0}\Big] + \sum_{i=2}^{k}\ln\Big[\frac{i}{i-1}\Big]\right)\right) \\
&\sim \mathcal{N}\left(0, \frac{2D}{\epsilon^2}\ln\left[\frac{1.25N}{\delta_0}\prod_{i=2}^{k}\frac{i}{i-1}\right]\right) \\
&\sim \mathcal{N}\left(0, \frac{2D}{\epsilon^2}\ln\Big[\frac{1.25kN}{\delta_0}\Big]\right) \\
&= \vec{\xi}_k^1. \qquad (27)
\end{aligned}$$

For the black-box scenario, where prior perturbations cannot be tracked, the cumulative noise at client k in the first round equals the sum of the per-client required noises. Using independence of the zero-mean Gaussian terms, the

variance parameters add:

$$\begin{aligned}\vec{\Xi}_k^1 &= \sum_{i=1}^{k} \vec{\xi}_i^1 \\ &\sim \mathcal{N}\left(0, \frac{2D}{\epsilon^2} \sum_{i=1}^{k} \ln\left[\frac{1.25\, i\, N}{\delta_0}\right]\right) \\ &\sim \mathcal{N}\left(0, \frac{2D}{\epsilon^2} \ln\left[\prod_{i=1}^{k} \frac{1.25\, i\, N}{\delta_0}\right]\right) \\ &\sim \mathcal{N}\left(0, \frac{2D}{\epsilon^2} \ln\left[\left(\frac{1.25\, N}{\delta_0}\right)^k\, k!\right]\right). \end{aligned} \tag{28}$$

Let $A = \frac{1.25\, N}{\delta_0} > 1$. The PrivateDFL variance factor for client k in round 1 is $\ln[kA]$, whereas the black-box factor is $k \ln A + \ln(k!) = \ln\big[(A)^k k!\big]$. Since

$$\ln\big[(A)^k k!\big] - \ln[kA] = (k-1)\ln A + \ln\big((k-1)!\big) > 0 \quad (k \geq 2),$$

the black-box cumulative noise is strictly larger than the PrivateDFL noise for all $k \geq 2$.

Aggregating the Gaussian increments from all K clients over the first $r-1$ rounds and from the first k clients in round r, and using telescoping of the logarithmic terms, we obtain the cumulative noise at client k in round r:

$$\begin{aligned}\vec{\gamma}_k^r &= \sum_{j=1}^{r-1} \sum_{i=1}^{K} \vec{\Gamma}_i^j \;+\; \sum_{i=1}^{k} \vec{\Gamma}_i^r \\ &\sim \mathcal{N}\Bigg(0, \frac{2D}{\epsilon^2}\Bigg[\ln\left[\tfrac{1.25N}{\delta_0}\right] + \sum_{i=2}^{K} \ln\left[\tfrac{i}{i-1}\right] + \sum_{t=K}^{2K-1} \ln\left[\tfrac{t+1}{t}\right] + \cdots \\ &\qquad + \sum_{t=K(r-2)+1}^{K(r-1)} \ln\left[\tfrac{t+1}{t}\right] + \sum_{t=K(r-1)}^{K(r-1)+k-1} \ln\left[\tfrac{t+1}{t}\right]\Bigg]\Bigg) \\ &\sim \mathcal{N}\Bigg(0, \frac{2D}{\epsilon^2} \ln\Bigg[\tfrac{1.25N}{\delta_0} \prod_{i=2}^{K} \tfrac{i}{i-1} \prod_{t=K}^{2K-1} \tfrac{t+1}{t} \cdots \\ &\qquad \prod_{t=K(r-2)+1}^{K(r-1)} \tfrac{t+1}{t} \prod_{t=K(r-1)}^{K(r-1)+k-1} \tfrac{t+1}{t}\Bigg]\Bigg) \\ &\sim \mathcal{N}\left(0, \frac{2D}{\epsilon^2} \ln\left[\frac{1.25\left(K(r-1)+k\right) N}{\delta_0}\right]\right) \\ &= \vec{\xi}_k^r. \end{aligned} \tag{29}$$

Setting $r = R$ and $k = K$ yields the final cumulative noise after R rounds and K clients; we define

$$\vec{\gamma}_K^R \sim \mathcal{N}\left(0,\; \frac{2D}{\epsilon^2}\; \ln\left[\frac{1.25\, KR\, N}{\delta_0}\right]\right), \tag{30}$$

which is the cumulative noise added to the HD model over R communication rounds by K clients to train the final secure model in the PrivateDFL algorithm.

We now derive the cumulative noise in the black-box scenario, where each client adds the full required noise $\vec{\xi}_k^r$ at every round without tracking what was already added in prior rounds. For client k at round r, the cumulative noise is

$$\begin{aligned}\vec{\Xi}_k^r = \vec{\xi}_1^1 + \vec{\xi}_2^1 + \cdots + \vec{\xi}_K^1 + \vec{\xi}_1^2 + \vec{\xi}_2^2 + \cdots + \vec{\xi}_K^2 + \cdots \\ + \vec{\xi}_1^{r-1} + \vec{\xi}_2^{r-1} + \cdots + \vec{\xi}_K^{r-1} + \vec{\xi}_1^r + \vec{\xi}_2^r + \cdots + \vec{\xi}_k^r. \end{aligned} \tag{31}$$

From Proof 4, the required noise for client i at round j is

$$\vec{\xi}_i^j \sim \mathcal{N}\left(0, \frac{2D}{\epsilon^2} \ln\left[\frac{1.25Nji}{\delta_0}\right]\right). \tag{32}$$

Substituting into the cumulative expression gives

$$\begin{aligned}\vec{\Xi}_k^r = &\mathcal{N}\left(0, \frac{2D}{\epsilon^2} \ln\left[\tfrac{1.25N}{\delta_0}\right]\right) + \mathcal{N}\left(0, \frac{2D}{\epsilon^2} \ln\left[\tfrac{1.25N\cdot 2}{\delta_0}\right]\right) + \cdots \\ &+ \mathcal{N}\left(0, \frac{2D}{\epsilon^2} \ln\left[\tfrac{1.25N\cdot K}{\delta_0}\right]\right) \\ &+ \mathcal{N}\left(0, \frac{2D}{\epsilon^2} \ln\left[\tfrac{1.25N\cdot (K+1)}{\delta_0}\right]\right) + \cdots \\ &+ \mathcal{N}\left(0, \frac{2D}{\epsilon^2} \ln\left[\tfrac{1.25N(K(r-1)+k)}{\delta_0}\right]\right).\end{aligned} \tag{33}$$

Collecting all terms, the cumulative noise at client k in round r becomes

$$\vec{\Xi}_k^r \sim \mathcal{N}\left(0, \frac{2D}{\epsilon^2}\left[\sum_{t=1}^{K(r-1)+k} \ln\left(\tfrac{1.25Nt}{\delta_0}\right)\right]\right). \tag{34}$$

This summation can be factorized into a product form:

$$\begin{aligned}\vec{\Xi}_k^r &\sim \mathcal{N}\left(0, \frac{2D}{\epsilon^2} \ln\left[\prod_{t=1}^{K(r-1)+k} \tfrac{1.25Nt}{\delta_0}\right]\right) \\ &= \mathcal{N}\left(0, \frac{2D}{\epsilon^2} \ln\left[\left(\tfrac{1.25N}{\delta_0}\right)^{K(r-1)+k} \times (K(r-1)+k)!\right]\right).\end{aligned} \tag{35}$$

Finally, setting $r = R$ and $k = K$, we obtain the total cumulative noise across R rounds and K clients:

$$\vec{\Xi}_K^R \sim \mathcal{N}\left(0, \frac{2D}{\epsilon^2} \ln\left[\left(\tfrac{1.25N}{\delta_0}\right)^{KR} \times (KR)!\right]\right). \tag{36}$$

This shows that in the black-box case the cumulative noise grows with $(KR)!$, which is significantly larger than the controlled logarithmic growth in PrivateDFL.

4 Experimental Design

We evaluate the effectiveness of PrivateDFL using three widely adopted benchmark datasets that span different modalities: MNIST (image-based), ISOLET (speech signal-based), and UCI-HAR (tabular sensor-based). This selection allows us to demonstrate the robustness of the proposed framework across heterogeneous data types. To assess data distribution effects, we consider both Independent and Identically Distributed (IID) and non-IID scenarios. In the IID case, data samples are divided uniformly across clients so that each client has an equal share of the global distribution. In contrast, the non-IID setting enforces data heterogeneity by restricting each client to only two classes; for instance, in MNIST, one client may receive only digits {0,1}, another {2,3}, and so on. This split reflects realistic IoT deployments where edge devices often collect skewed data.

Our evaluation follows a stepwise methodology. First, we conduct a sensitivity analysis to investigate how privacy parameters and HD model configurations influence PrivateDFL performance. We report accuracy and examine its dependence on the privacy budget ϵ and privacy loss parameter δ, the hypervector dimensionality D, and the number

of training samples per client under both IID and non-IID partitions. For the IID setting, we also vary the number of clients K while keeping the total training data fixed, which isolates the effect of partitioning and highlights the trade off between coordination and performance.

Beyond internal sensitivity studies, we benchmark PrivateDFL against state-of-the-art Transformer-based and deep learning models trained with DP in centralized settings. These baseline models operate without federated constraints, accessing the complete dataset directly, and therefore represent the upper bound of achievable accuracy with minimal latency. We implement two privacy mechanisms, DP-SGD and RDP, using the Opacus library for PyTorch [49]. For MNIST, we benchmark against vision architectures including Vision Transformer, ResNet50, GoogLeNet, and AlexNet. For ISOLET, we employ sequential models such as Transformer, Convolutional Neural Network (CNN), Recurrent Neural Network (RNN), and Temporal Convolutional Network (TCN). For UCI-HAR, we adopt tabular learning architectures including TabTransformer, TabNet, Deep Neural Network (DNN), and Deep and Cross Network (DCN). Comparisons are reported in terms of accuracy, training time, energy consumption, and inference latency, under a fixed privacy budget of $\epsilon = 0.4$ and a privacy loss coefficient of $\delta_0 = 0.001$.

All experiments are conducted in a controlled computing environment configured to emulate the constraints of edge devices while ensuring reproducibility. Each system is equipped with dual 32-core AMD EPYC 7513 processors, 512 GB of RAM, fast SSD storage, and an NVIDIA A100 GPU with 40 GB of memory, 6912 CUDA cores, and 1.6 TB/s memory bandwidth. While the hardware enables precise measurement of performance metrics, our optimization framework enforces strict limits on latency and energy consumption to mirror practical IoT scenarios. Random seeds are fixed for all runs, and energy and timing are recorded directly at the training and inference stages to provide accurate performance assessments.

5 Experimental Results

5.1 Sensitivity Analysis

In this subsection, we examine how key hyperparameters including the privacy budget ϵ, the privacy loss parameter δ_0, the number of clients K, the hypervector dimensionality D, and the number of training samples per client affect PrivateDFL accuracy. We begin with the privacy parameters under an IID split.

Figure 5a shows test accuracy on MNIST when the training data are evenly partitioned across 100 clients under IID conditions. With a large privacy budget (for example, $\epsilon = 1$ and $\delta_0 = 10^{-3}$), the injected noise is small and accuracy reaches 96.34%. Fixing $\delta_0 = 10^{-9}$ and decreasing ϵ increases the noise magnitude and reduces accuracy; the curve drops from 96.14% at $\epsilon = 1$ to 95.62%, 94.23%, 93.65%, 89.78%, 87.32%, and 75.16% at $\epsilon \in \{0.5, 0.1, 0.05, 0.01, 0.005, 0.001\}$.

By contrast, varying δ_0 has only a marginal effect. For instance, at $\epsilon = 0.1$, tightening δ_0 from 10^{-3} to 10^{-18} changes accuracy by about 0.56 percentage points (from 94.53% to 93.97%). Small fluctuations also appear due to randomness in noise draws across repeated runs; for example, at $\epsilon = 0.5$ the accuracy is 95.49% for $\delta_0 = 10^{-12}$, 95.62% for $\delta_0 = 10^{-9}$, and 95.76% for $\delta_0 = 10^{-15}$, which is a difference of at most 0.27 percentage points. The same trends hold for ISOLET and UCI-HAR under IID conditions with 100 clients, as shown in Figures 5b and 5c.

Figs. 5d, 5e, and 5f extend this analysis to the non-IID setting, continuing the trends observed under IID while revealing stronger sensitivity for MNIST due to client heterogeneity. At $\epsilon = 0.5$ and $\delta_0 = 10^{-6}$, MNIST accuracy declines from 95.81% under IID to 89.08% under non-IID. ISOLET and UCI-HAR show smaller gaps under the same parameters, with 88.01% versus 89.22% for ISOLET and 93.99% versus 92.09% for UCI-HAR.

Figure 6 extends the analysis by reporting accuracy as a function of the number of clients under IID partitioning for MNIST, ISOLET, and UCI-HAR across communication rounds. We vary K from 10 to 1000 while keeping the total training set fixed and evenly distributed, so any change in performance reflects the effect of partitioning and coordination rather than data volume. For each round, the plot summarizes the mean accuracy across client counts together with the standard deviation. The variability is small for MNIST, remaining below 1.5%, moderate for ISOLET, reaching up to 5.31%, and larger for UCI-HAR, reaching up to 7.37%. The standard deviation is nearly constant from round to round within each dataset, indicating that uncertainty is driven primarily by the dataset and task rather than the communication round.

Complementing the client-count study in Figure 6, Figure 7 presents the effect of hypervector dimensionality and the number of training samples per client on model accuracy. Figs. 7a, 7b, and 7c correspond to the MNIST, ISOLET, and UCI-HAR datasets, respectively, with hypervector sizes varied from 50 to 500 and training samples per client from 50 to 250 for MNIST, and from 5 to 25 for ISOLET and UCI-HAR.

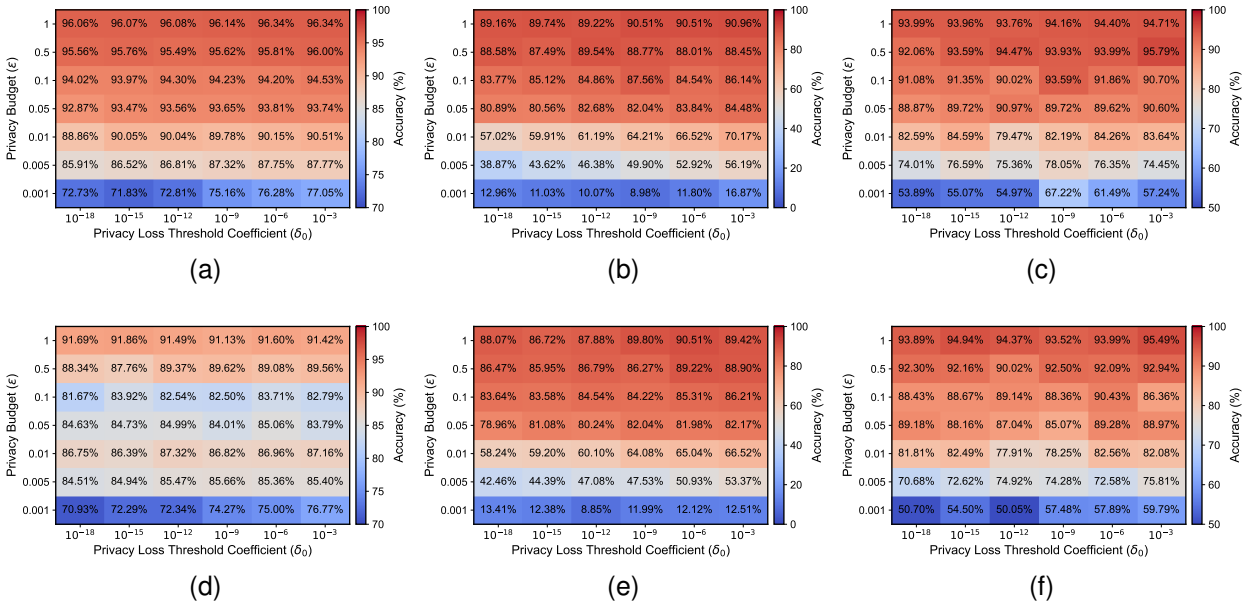

Figure 5: Model accuracy trends under varying privacy budget (ε) and privacy loss coefficient (δ_0) values for IID and non-IID scenarios. (a)–(c) correspond to IID distributions for MNIST, ISOLET, and UCI-HAR datasets, respectively. (d)–(f) show the results under non-IID distributions for the same datasets.

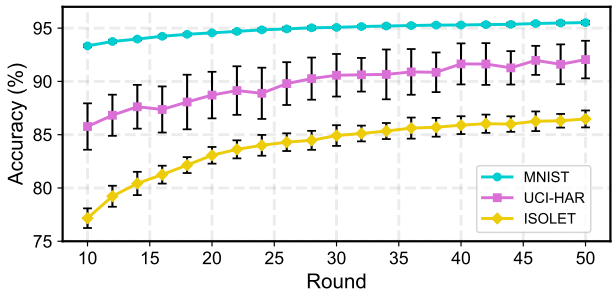

Figure 6: Three curves show MNIST, ISOLET, and UCI-HAR accuracy across communication rounds, with each round's marker giving the mean over $K \in \{10, \ldots, 1000\}$ and the shaded band indicating ±1 standard deviation across those K values.

For the MNIST dataset, accuracy depends strongly on hypervector size. For instance, with 200 training samples, accuracy improves steadily from 65.35% to 91.86% as hypervector size increases from 50 to 500. Conversely, when hypervector size is fixed at 300, accuracy increases more gradually from 86.68% to 92.27% as the number of training samples grows from 50 to 250. This indicates that hypervector dimensionality has a stronger influence on MNIST performance than the number of samples.

For ISOLET, the trend is reversed: accuracy is more sensitive to the number of training samples than to hypervector size. For example, when the hypervector size is fixed at 500, accuracy improves from 53.56% to 77.99% as the number of training samples per client increases from 5 to 25. However, for a fixed training size, enlarging the hypervector dimension has only a marginal effect. At 5 training samples per client, accuracy increases by 5.70% when hypervector size increases from 50 to 500, and at 25 training samples the increase is 8.53%.

The UCI-HAR dataset follows the same pattern as ISOLET, where accuracy is more dependent on training data size than on hypervector dimensionality. With hypervector size fixed at 50, accuracy increases by 12.04% as training samples per client grow from 5 to 25. When the hypervector size is 500, the increase is 14.86%. However, once clients already have 25 samples each, further increasing hypervector dimensionality yields only a modest 1.05% accuracy increase. These results highlight that for ISOLET and UCI-HAR, additional data availability is more beneficial than expanding hypervector size.

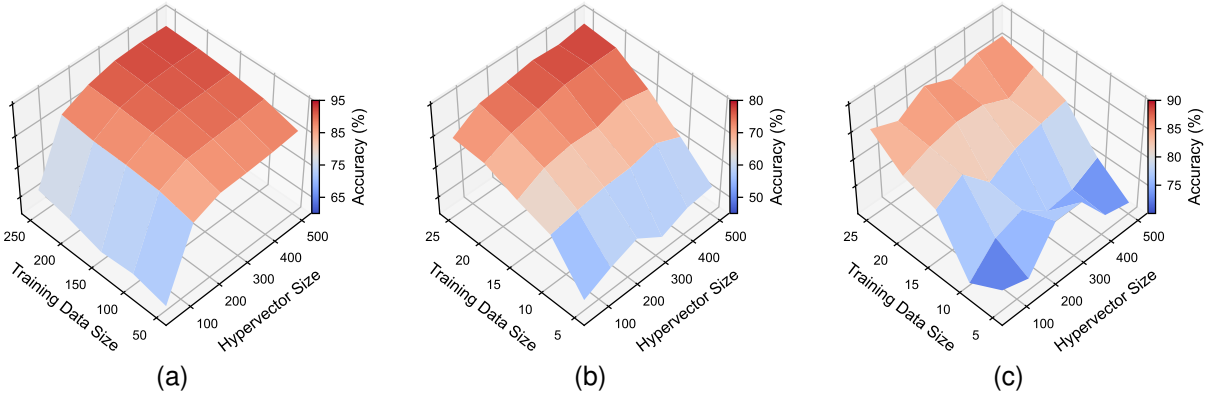

Figure 7: Impact of the number of training samples per client and hypervector size on model performance under IID settings. Subfigures (a)–(c) show classification accuracy for MNIST, ISOLET, and UCI-HAR datasets, respectively.

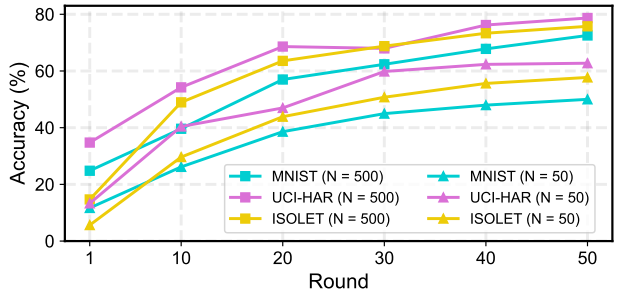

Figure 8: Accuracy of PrivateDFL over communication rounds for different portions of training samples on the non-IID datasets.

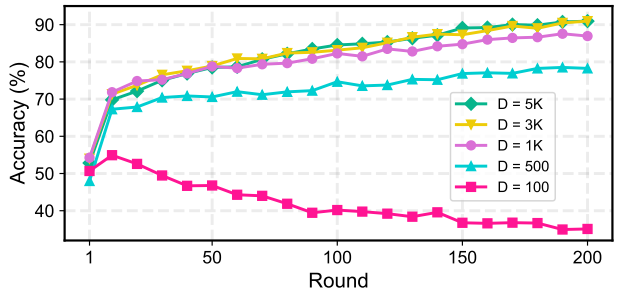

Figure 9: Accuracy of PrivateDFL over communication rounds for different hypervector dimensions (D) on the non-IID MNIST dataset.

Extending to the non-IID scenario, Figure 8 reports accuracy across communication rounds while varying the number of training samples per client. For MNIST with 50 samples per client, accuracy starts at 11.68% in round 1 and reaches 50.00% by round 50. Increasing the sample count raises accuracy at every round; for example, the first–round accuracy rises to 24.81% and the round–50 accuracy reaches 72.53% when more training samples are available. The same upward trend holds for ISOLET and UCI-HAR: after 50 rounds, accuracy is 57.72% and 62.74% with 50 samples per client, and increases to 75.75% and 78.69% when each client has 500 samples. Across the tested hypervector sizes, the effect of adding training samples dominates, producing consistent gains under non-IID partitions.

Finally, Figure 9 examines the effect of hypervector dimensionality under non-IID partitions for MNIST. Accuracy at round 1 is close to 50% for all tested sizes. For a very small dimension such as $D = 100$, the model lacks capacity to retain class information and the injected DP noise dominates, so accuracy decreases as rounds proceed; at rounds 50, 100, 150, and 200, the values are 46.78%, 40.18%, 36.76%, and 35.10%. Increasing D counteracts this effect. With

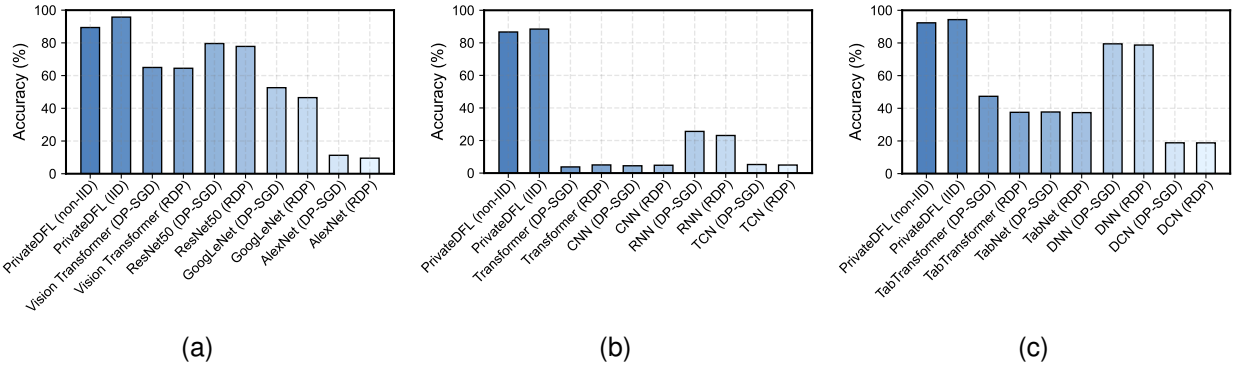

Figure 10: Comparison of accuracy between PrivateDFL and baseline ML models with DP across datasets. (a) MNIST, (b) ISOLET, and (c) UCI-HAR.

$D = 500$, accuracy improves across rounds, reaching 70.57%, 74.66%, 76.86%, and 78.25% at rounds 50, 100, 150, and 200. Larger dimensions provide further gains: after 200 rounds, accuracy is 86.93% for $D = 1000$ and 90.95% for $D = 3000$, which are increases of 8.68% and 12.70% relative to $D = 500$ at the same round. Beyond this range, returns diminish because larger D also increases the effective noise scale; for $D = 5000$, the round 200 accuracy is 90.94%, essentially the same as for $D = 3000$.

5.2 Benchmark

Figure 10 compares PrivateDFL with differentially private ML baselines across MNIST, ISOLET, and UCI-HAR under IID and non-IID partitions. Across datasets, PrivateDFL consistently delivers the strongest accuracy while meeting the same privacy budgets.

For MNIST (Figure 10a), PrivateDFL attains 95.74% in IID and 89.38% in non-IID. DP regularized deep models lag well behind. AlexNet reaches 11.27% with DP-SGD and 9.51% with RDP, GoogLeNet achieves 52.60% and 46.53%, ResNet50 reaches 79.59% and 77.83%, and Vision Transformer reaches 64.96% and 64.47%. These outcomes indicate that the hyperdimensional backbone of PrivateDFL preserves utility more effectively under privacy noise.

For ISOLET (Figure 10b), PrivateDFL leads with 88.45% in IID and 86.66% in non-IID. Transformer and CNN baselines trained with DP remain between 3.78% and 5.26%. RNN yields 25.59% with DP-SGD and 23.09% with RDP, while TCN stays below 6%. The pronounced gap shows that sequential deep models are highly sensitive to DP noise, whereas PrivateDFL sustains strong accuracy.

For UCI-HAR (Figure 10c), PrivateDFL reaches 94.30% in IID and 92.33% in non-IID. Among tabular baselines, TabTransformer attains 47.34% with DP-SGD and 37.53% with RDP, TabNet yields 37.73% and 37.36%, DNN reaches 79.47% and 78.72%, and DCN is near 18.87% and 18.83%. Taken together, these results show that PrivateDFL balances privacy and utility more effectively than conventional ML with DP across image, speech, and sensor modalities.

Building on the accuracy gains in Figure 10, Figure 11 compares training time and inference latency for PrivateDFL and differentially private baselines on MNIST, ISOLET, and UCI-HAR under IID and non-IID partitions. The results show that the utility advantages of PrivateDFL come with substantially lower runtime.

For MNIST in Figures 11a and 11d, PrivateDFL trains in 820.97 seconds for IID and 730.81 seconds for non-IID. Deep baselines are far slower. GoogLeNet requires 23127.31 seconds with DP-SGD and 21545.07 seconds with RDP. ResNet50 requires 21656.82 and 21768.85 seconds. AlexNet exceeds 16000 seconds, and Vision Transformer requires between 7684.12 and 8384.22 seconds. At inference, PrivateDFL reaches 11.16 milliseconds, while the deep models range from 756 to 1338 milliseconds. These findings are consistent with the accuracy comparison and indicate a favorable speed–utility profile on image data.

For ISOLET in Figures 11b and 11e, PrivateDFL trains in 311.71 seconds for IID and 79.60 seconds for non-IID. RNN baselines with DP require more than 1680 seconds, TCN requires more than 1820 seconds, and Transformer requires more than 800 seconds. Inference latency widens the gap. PrivateDFL completes inference in 1.98 milliseconds, whereas sequential baselines require from 83 to 216 milliseconds. These outcomes show that PrivateDFL scales efficiently for speech like signals under the same privacy requirements.

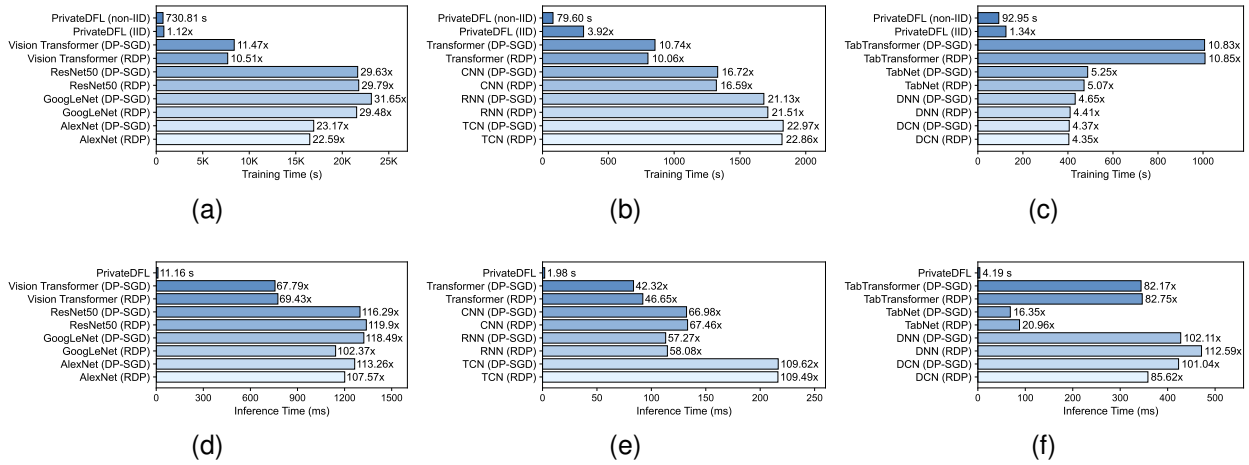

Figure 11: Comparison of training time (top row) and inference latency (bottom row) between PrivateDFL and baseline ML models with DP. (a,d) MNIST, (b,e) ISOLET, and (c,f) UCI-HAR.

For UCI-HAR in Figures 11c and 11f, PrivateDFL trains in 124.85 seconds for IID and 92.95 seconds for non-IID. TabTransformer requires about 1007 seconds, TabNet requires about 480 seconds, and both DNN and DCN exceed 400 seconds. At inference, PrivateDFL achieves 4.19 milliseconds, while TabTransformer requires 344 to 346 milliseconds, DNN requires 428 to 471 milliseconds, and TabNet requires 68 to 88 milliseconds. Together with the accuracy results in Figure 10c, this confirms that PrivateDFL maintains strong utility for sensor data with markedly lower runtime.

These timing results complement the accuracy analysis and motivate the energy evaluation that follows, where we examine whether the same advantages persist in power constrained deployments.

Building on the runtime analysis, Figure 12 reports energy use for PrivateDFL and differentially private baselines on MNIST, ISOLET, and UCI-HAR under IID and non-IID partitions. The pattern mirrors the time and accuracy results. PrivateDFL reaches the same privacy budgets at much lower energy cost.

For MNIST in Figure 12a, PrivateDFL consumes 0.03 MJ for IID and 0.03 MJ for non-IID. ResNet50 requires 3.97 MJ with DP-SGD and 3.99 MJ with RDP. AlexNet is about 3.6 MJ. GoogLeNet ranges from 1.29 to 1.33 MJ. Vision Transformer uses 0.33 MJ. Thus, PrivateDFL delivers comparable image accuracy while consuming at least 11× less energy than the most efficient deep baseline (Vision Transformer at 0.33 MJ) and up to about 130× less than ResNet50 and 120× less than AlexNet, and under non-IID the savings are unchanged since PrivateDFL remains at 0.03 MJ.

For ISOLET in Figure 12b, PrivateDFL records 12.32 kJ for IID and 3.43 kJ for non-IID. CNN requires about 330 kJ, TCN exceeds 450 kJ, and Transformer models are between 124 and 130 kJ. Even RNNs require 65 to 67 kJ. Overall, PrivateDFL attains strong speech recognition accuracy while consuming at least 5× less energy than the most efficient deep baseline (RNN at 65–67 kJ) and up to about 130× less than TCN and CNN, and under non-IID partitions the savings are even larger with 3.43 kJ for PrivateDFL which is at least 19× below the most efficient deep baseline and up to roughly 130× below TCN and about 100× below CNN.

For UCI-HAR in Figure 12c, PrivateDFL consumes 4.96 kJ for IID and 3.50 kJ for non-IID. TabTransformer is near 248 kJ. TabNet requires 18 to 21 kJ. DNNs require 28 to 34 kJ, and DCN is about 20 to 22 kJ. PrivateDFL therefore offers the most energy-efficient solution for sensor data among the evaluated methods.

Overall, the energy evaluation complements the accuracy and time results. PrivateDFL sustains high utility while markedly lowering energy across all three modalities, which makes it well-suited for resource-constrained IoT and edge deployments.

6 Conclusions and Future Work

This work introduced *PrivateDFL*, a privacy-aware DFL framework that couples HD with differentially private noise control and explainable accounting. The method provides three complementary properties. First, interpretability through high-dimensional class prototypes and transparent update rules. Second, formal privacy via calibrated Gaussian noise

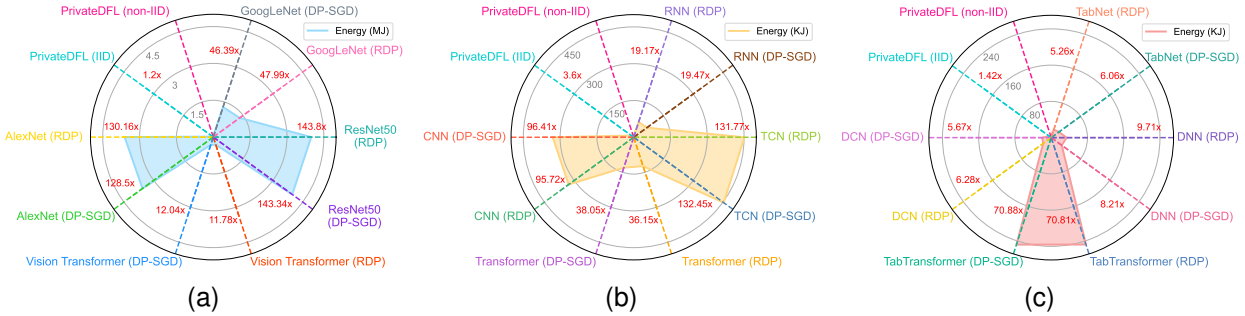

Figure 12: Energy consumption comparison between PrivateDFL and baseline ML models with DP across datasets. (a) MNIST, (b) ISOLET, and (c) UCI-HAR.

with closed-form schedules proven for each client and round. Third, practicality on resource-constrained devices due to lightweight operations and low communication overhead.

When comparing against baselines, it is important to note that those models are trained centrally without federated constraints. They access the entire dataset directly and therefore represent an upper bound on achievable accuracy with minimal latency. Even under this favorable setting for the baselines, PrivateDFL attains strong utility. On image, speech, and sensor tasks, PrivateDFL reaches 95.74% on MNIST, 88.45% on ISOLET, and 94.30% on UCI-HAR under IID partitioning, with similar trends under non-IID. The gains are substantial. Relative to transformer models the accuracy advantage is as large as about 83% on ISOLET and about 31% on MNIST, and relative to deep learning models the advantage is as large as about 63% on ISOLET and about 16% on MNIST, while on UCI-HAR, PrivateDFL exceeds the strongest tabular baseline by about 15%. These improvements come together with markedly lower training time and energy usage across all three modalities, which makes PrivateDFL a compelling choice for edge and IoT deployments.

PrivateDFL has limitations that motivate future work. First, we assumed synchronous ring-style communication and reliable message passing. Extending the noise accounting and proofs to asynchronous schedules, dynamic topologies, and client churn is an open direction. Second, we used a uniform privacy target across clients and classes. Adapting (ϵ, δ) to local data difficulty or risk, while preserving end-to-end guarantees, may further improve the privacy-utility balance. Third, robustness to adversaries warrants deeper study, including targeted data poisoning, backdoor insertion, and stronger inference attacks under heterogeneous participation. Fourth, additional secure computation layers such as secure aggregation, lightweight homomorphic encryption, or verifiable computation could be integrated to harden the protocol without sacrificing efficiency.

In summary, PrivateDFL demonstrates that interpretable hyperdimensional models, decentralized training, and explainable DP can jointly deliver high accuracy, strong privacy, and low cost. We believe these results chart a path toward trustworthy, scalable, and energy-efficient federated intelligence at the network edge.

Acknowledgments

This work was supported by the National Science Foundation, United States [grant number 2434519].

Supplementary Materials

The code used in this study is openly available for reproducibility and can be accessed at the following link: https://github.com/FardinJalilPiran/PrivateDFL.git.

References

[1] Chao Liu, Boxi Chen, Wei Shao, Chris Zhang, Kelvin KL Wong, and Yi Zhang. Unraveling attacks to machine learning-based iot systems: A survey and the open libraries behind them. *IEEE Internet of Things Journal*, 2024.

[2] Chengcheng Wang, Xipeng P Tan, Shu Beng Tor, and CS Lim. Machine learning in additive manufacturing: State-of-the-art and perspectives. *Additive Manufacturing*, 36:101538, 2020.

[3] Sweta Bhattacharya, Siva Rama Krishnan Somayaji, Thippa Reddy Gadekallu, Mamoun Alazab, and Praveen Kumar Reddy Maddikunta. A review on deep learning for future smart cities. *Internet Technology Letters*, 5(1):e187, 2022.

[4] Tengchan Zeng, Omid Semiari, Mingzhe Chen, Walid Saad, and Mehdi Bennis. Federated learning on the road autonomous controller design for connected and autonomous vehicles. *IEEE Transactions on Wireless Communications*, 21(12):10407–10423, 2022.

[5] Yaohua Sun, Mugen Peng, Yangcheng Zhou, Yuzhe Huang, and Shiwen Mao. Application of machine learning in wireless networks: Key techniques and open issues. *IEEE Communications Surveys & Tutorials*, 21(4):3072–3108, 2019.

[6] Dinh C Nguyen, Ming Ding, Pubudu N Pathirana, Aruna Seneviratne, Jun Li, and H Vincent Poor. Federated learning for internet of things: A comprehensive survey. *IEEE Communications Surveys & Tutorials*, 23(3):1622–1658, 2021.

[7] Nuria Rodríguez-Barroso, Daniel Jiménez-López, M Victoria Luzón, Francisco Herrera, and Eugenio Martínez-Cámara. Survey on federated learning threats: Concepts, taxonomy on attacks and defences, experimental study and challenges. *Information Fusion*, 90:148–173, 2023.

[8] Liangqi Yuan, Ziran Wang, Lichao Sun, S Yu Philip, and Christopher G Brinton. Decentralized federated learning: A survey and perspective. *IEEE Internet of Things Journal*, 2024.

[9] Matt Fredrikson, Somesh Jha, and Thomas Ristenpart. Model inversion attacks that exploit confidence information and basic countermeasures. In *Proceedings of the 22nd ACM SIGSAC conference on computer and communications security*, pages 1322–1333, 2015.

[10] Reza Shokri, Marco Stronati, Congzheng Song, and Vitaly Shmatikov. Membership inference attacks against machine learning models. In *2017 IEEE symposium on security and privacy (SP)*, pages 3–18. IEEE, 2017.

[11] Yoshinori Aono, Takuya Hayashi, Lihua Wang, Shiho Moriai, et al. Privacy-preserving deep learning via additively homomorphic encryption. *IEEE transactions on information forensics and security*, 13(5):1333–1345, 2017.

[12] Qiang Zhu and Xixiang Lv. 2p-dnn: Privacy-preserving deep neural networks based on homomorphic cryptosystem. *arXiv preprint arXiv:1807.08459*, 2018.

[13] D Apple. Learning with privacy at scale. *Apple Machine Learning Journal*, 1(8):71, 2017.

[14] Xiaofeng Ding, Cui Wang, Kim-Kwang Raymond Choo, and Hai Jin. A novel privacy preserving framework for large scale graph data publishing. *IEEE transactions on knowledge and data engineering*, 33(2):331–343, 2019.

[15] Úlfar Erlingsson, Vasyl Pihur, and Aleksandra Korolova. Rappor: Randomized aggregatable privacy-preserving ordinal response. In *Proceedings of the 2014 ACM SIGSAC conference on computer and communications security*, pages 1054–1067, 2014.

[16] Edwige Cyffers and Aurélien Bellet. Privacy amplification by decentralization. In *International Conference on Artificial Intelligence and Statistics*, pages 5334–5353. PMLR, 2022.

[17] Muah Kim, Onur Günlü, and Rafael F Schaefer. Federated learning with local differential privacy: Trade-offs between privacy, utility, and communication. In *ICASSP 2021-2021 IEEE International Conference on Acoustics, Speech and Signal Processing (ICASSP)*, pages 2650–2654. IEEE, 2021.

[18] Hanchi Ren, Jingjing Deng, and Xianghua Xie. Grnn: generative regression neural network—a data leakage attack for federated learning. *ACM Transactions on Intelligent Systems and Technology (TIST)*, 13(4):1–24, 2022.

[19] Nazish Khalid, Adnan Qayyum, Muhammad Bilal, Ala Al-Fuqaha, and Junaid Qadir. Privacy-preserving artificial intelligence in healthcare: Techniques and applications. *Computers in Biology and Medicine*, 158:106848, 2023.

[20] Tian Li, Anit Kumar Sahu, Ameet Talwalkar, and Virginia Smith. Federated learning: Challenges, methods, and future directions. *IEEE signal processing magazine*, 37(3):50–60, 2020.

[21] Wenzhi Fang, Yuning Jiang, Yuanming Shi, Yong Zhou, Wei Chen, and Khaled B Letaief. Over-the-air computation via reconfigurable intelligent surface. *IEEE transactions on communications*, 69(12):8612–8626, 2021.

[22] Ahmed Imteaj, Urmish Thakker, Shiqiang Wang, Jian Li, and M Hadi Amini. A survey on federated learning for resource-constrained iot devices. *IEEE Internet of Things Journal*, 9(1):1–24, 2021.

[23] Chuan Ma, Jun Li, Ming Ding, Howard H Yang, Feng Shu, Tony QS Quek, and H Vincent Poor. On safeguarding privacy and security in the framework of federated learning. *IEEE network*, 34(4):242–248, 2020.

[24] Eugene Bagdasaryan, Andreas Veit, Yiqing Hua, Deborah Estrin, and Vitaly Shmatikov. How to backdoor federated learning. In *International conference on artificial intelligence and statistics*, pages 2938–2948. PMLR, 2020.

[25] Vale Tolpegin, Stacey Truex, Mehmet Emre Gursoy, and Ling Liu. Data poisoning attacks against federated learning systems. In *Computer security–ESORICs 2020: 25th European symposium on research in computer security, ESORICs 2020, guildford, UK, September 14–18, 2020, proceedings, part i 25*, pages 480–501. Springer, 2020.

[26] Anusha Lalitha, Shubhanshu Shekhar, Tara Javidi, and Farinaz Koushanfar. Fully decentralized federated learning. In *Third workshop on bayesian deep learning (NeurIPS)*, volume 12, 2018.

[27] Xiangru Lian, Ce Zhang, Huan Zhang, Cho-Jui Hsieh, Wei Zhang, and Ji Liu. Can decentralized algorithms outperform centralized algorithms? a case study for decentralized parallel stochastic gradient descent. *Advances in neural information processing systems*, 30, 2017.

[28] Youyang Qu, Longxiang Gao, Tom H Luan, Yong Xiang, Shui Yu, Bai Li, and Gavin Zheng. Decentralized privacy using blockchain-enabled federated learning in fog computing. *IEEE Internet of Things Journal*, 7(6):5171–5183, 2020.

[29] Cynthia Dwork, Aaron Roth, et al. The algorithmic foundations of differential privacy. *Foundations and trends® in theoretical computer science*, 9(3–4):211–407, 2014.

[30] Martin Abadi, Andy Chu, Ian Goodfellow, H Brendan McMahan, Ilya Mironov, Kunal Talwar, and Li Zhang. Deep learning with differential privacy. In *Proceedings of the 2016 ACM SIGSAC conference on computer and communications security*, pages 308–318, 2016.

[31] Ilya Mironov. Rényi differential privacy. In *2017 IEEE 30th computer security foundations symposium (CSF)*, pages 263–275. IEEE, 2017.

[32] Maoguo Gong, Jialun Feng, and Yu Xie. Privacy-enhanced multi-party deep learning. *Neural Networks*, 121:484–496, 2020.

[33] Huiwen Wu, Cen Chen, and Li Wang. A theoretical perspective on differentially private federated multi-task learning. *arXiv preprint arXiv:2011.07179*, 2020.

[34] Ahmed El Ouadrhiri and Ahmed Abdelhadi. Differential privacy for deep and federated learning: A survey. *IEEE access*, 10:22359–22380, 2022.

[35] Anh-Tu Tran, The-Dung Luong, Jessada Karnjana, and Van-Nam Huynh. An efficient approach for privacy preserving decentralized deep learning models based on secure multi-party computation. *Neurocomputing*, 422:245–262, 2021.

[36] Bin Zhao, Kai Fan, Kan Yang, Zilong Wang, Hui Li, and Yintang Yang. Anonymous and privacy-preserving federated learning with industrial big data. *IEEE Transactions on Industrial Informatics*, 17(9):6314–6323, 2021.

[37] Lihua Yin, Jiyuan Feng, Hao Xun, Zhe Sun, and Xiaochun Cheng. A privacy-preserving federated learning for multiparty data sharing in social iots. *IEEE Transactions on Network Science and Engineering*, 8(3):2706–2718, 2021.

[38] Tianchong Gao, Hailong Fu, Shunwei Wang, and Niu Zhang. Amoue: Adaptive modified optimized unary encoding method for local differential privacy data preservation. *Computers and Electrical Engineering*, 120:109791, 2024.

[39] Santanu Basak, Kakali Chatterjee, and Ashish Singh. Dppt: A differential privacy preservation technique for cyber–physical system. *Computers and Electrical Engineering*, 109:108661, 2023.

[40] Waqas Ali, Mohammad Nauman, and Nouman Azam. A privacy enhancing model for internet of things using three-way decisions and differential privacy. *Computers and Electrical Engineering*, 100:107894, 2022.

[41] Guiping Zheng, Bei Gong, Chong Guo, Tianqi Peng, and Mowei Gong. Awe-dpfl: Adaptive weighting and dynamic privacy budget federated learning for heterogeneous data in iot. *Computers and Electrical Engineering*, 123:110070, 2025.

[42] Alejandro Hernández-Cano, Rosario Cammarota, and Mohsen Imani. Prid: Model inversion privacy attacks in hyperdimensional learning systems. In *2021 58th ACM/IEEE Design Automation Conference (DAC)*, pages 553–558. IEEE, 2021.

[43] Behnam Khaleghi, Mohsen Imani, and Tajana Rosing. Prive-hd: Privacy-preserved hyperdimensional computing. In *2020 57th ACM/IEEE Design Automation Conference (DAC)*, pages 1–6. IEEE, 2020.

[44] Fardin Jalil Piran, Prathyush P Poduval, Hamza Errahmouni Barkam, Mohsen Imani, and Farhad Imani. Explainable differential privacy-hyperdimensional computing for balancing privacy and transparency in additive manufacturing monitoring. *Engineering Applications of Artificial Intelligence*, 147:110282, 2025.

[45] Fardin Jalil Piran, Zhiling Chen, Mohsen Imani, and Farhad Imani. Privacy-preserving federated learning with differentially private hyperdimensional computing. *Computers and Electrical Engineering*, 123:110261, 2025.

[46] Fardin Jalil Piran, Hamza Errahmouni Barkam, Mohsen Imani, and Farhad Imani. Hyperdimensional cognitive computing for lightweight cyberattack detection in industrial internet of things. In *Proceedings of the ASME 2023 International Design Engineering Technical Conferences and Computers and Information in Engineering Conference*, volume 7 of *19th IEEE/ASME International Conference on Mechatronic and Embedded Systems and Applications (MESA)*, page V007T07A013. American Society of Mechanical Engineers, 2023.

[47] Zhiling Chen, Danny Hoang, Fardin Jalil Piran, Ruimin Chen, and Farhad Imani. Federated hyperdimensional computing for hierarchical and distributed quality monitoring in smart manufacturing. *Internet of Things*, 31:101568, 2025.

[48] Fardin Jalil Piran, Prathyush P Poduval, Hamza Errahmouni Barkam, Mohsen Imani, and Farhad Imani. Privacy-preserving in-situ monitoring in additive manufacturing through hyperdimensional computing. In *ASME International Mechanical Engineering Congress and Exposition*, volume 88605, page V002T03A078. American Society of Mechanical Engineers, 2024.

[49] Ashkan Yousefpour, Igor Shilov, Alexandre Sablayrolles, Davide Testuggine, Karthik Prasad, Mani Malek, John Nguyen, Sayan Ghosh, Akash Bharadwaj, Jessica Zhao, et al. Opacus: User-friendly differential privacy library in pytorch. *arXiv preprint arXiv:2109.12298*, 2021.